Volume 1 | Number 1 | Jan 2013 | Pages 1–100

Journal of
Materials Chemistry A

Materials for energy and sustainability
www.rsc.org/materialsA

Li+
e−
e−
Li+
e−
Li+
Li+

ROYAL SOCIETY
OF CHEMISTRY

ROYAL SOCIETY
OF CHEMISTRY

www.rsc.org/materialsA

A table of contents entry
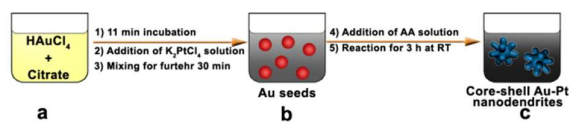
Well-dispersed, core-shell Au-Pt nanodendrites were synthesized *via* overgrowth of platinum on *in situ* 5.5 nm gold nanoparticles at room temperature.

ARTICLE TYPE

Synthesis of Core-Shell Au-Pt Nanodendrites with High Catalytic Performance *via* Overgrowth of Platinum on *in situ* Gold Nanoparticles

Yijing Li,[a] Wenchao Ding,[a] Mingrui Li,[a] Haibing Xia,[a,] Dayang Wang[b] and Xutang Tao[a]*

We present a simple and effective strategy for high yield synthesis of well-dispersed, core-shell Au-Pt nanodendrites (CS Au-Pt NDs) *via* overgrowth of platinum on *in situ* 5.5 nm gold nanoparticles in water at room temperature. The sizes of the resulting CS Au-Pt NDs are 14 nm, which should be the smallest so far to our best knowledge. The average dimension of the small Pt branches on the Au nanoparticle
10 surfaces is about 2.6 nm × 4.2 nm, which leads to significantly increased electrochemically active surface area (up to 35.2 m^2 g^{-1}). It is found that the morphology of CS Au-Pt NDs is dependent on the reaction conditions such as incubation time of citrate-HAuCl$_4$ solution, the mixing time of citrate-HAuCl$_4$-K$_2$PtCl$_4$ solution before AA addition, and Pt-to-Au and AA-to-Pt molar ratios. In comparison with commercial Pt black (0.12 A mg$_{Pd}^{-1}$), the resulting Au-Pt$_5$ NDs show superior catalytic activity towards methanol
15 oxidation (0.45 A mg$_{Pd}^{-1}$) due to the electronic interaction between the Au cores and Pt branches in bimetallic Au-Pt NDs and the high fraction of atomic steps, kinks, and corner atoms on the surfaces of the Pt branches.

1 Introduction

Due to the high cost and scarcity of Pt resources, the current
20 studies have focused on reduction of the Pt mass loading and improvement of the Pt utilization.[1-3] These goals can be achieved by optimization of the structures of Pt and Pt-based catalysts.[2-6] Typical parameters to tailor the catalytic performance are the composition, size, and morphology, respectively, of the Pt-based
25 catalysts. The composition, including the constituent elements (Pt and other metals) and their ratios, determines the basic essence of the Pt-based catalysts. The size determines the specific surface area and the ratio of surface to bulk atoms in the catalysts. The morphology (including shape and interface/surface engineering)
30 controls the fractions of atoms at the corners and edges of the catalysts. It is known that the introduction of other metals to form bimetallic Pt-based catalysts is the most promising strategy to implement superior catalytic activity owing to electronic effects.[7] For instance, foreign metals can alter the electronic properties of
35 Pt and lower the adsorption energy of CO, thereby facilitating the oxidation of CO at lower potentials. In addition, Pt-based catalysts with core–shell structures can greatly reduce the Pt utilization as the majority of Pt atoms are distributed at the electrochemical reaction interface.[8] The structure and properties
40 of the Pt shells can be finely manipulated by the core materials, owing to structure-induced strain (geometry) and electronic effects (alloying). For example, the existence of subsurface Au atoms may provide an additional contribution to the durability enhancement of the Pt skin layer by modifying the well-known
45 core-hindered place-exchange mechanism.[8,9]

Up to date, high-quality Pt-based catalysts with different shapes, including nanodendrites (NDs),[10] nanotubes,[4,11] nanopolyhedron,[12] nanocages,[13] nanowires[14] and so on, have been synthesized. Among them, non-compact small spikes structures
50 can reduce the overlaps during deposition, thus enable the catalytically active surface area to remain high and more high-index facets to be exposed and thus supply more active sites.[15-17] Yamauchi group have prepared monometallic,[15,16,18] bimetallic (Pd-Pt and Au-Pt),[19-21] and trimetallic (Au-Pd-Pt)[22] Pt particles
55 with multiple nanobranches, showing highly active electrocatalysts. Recently core-shell (CS) NDs with Au cores decorated with Pt nanobranches atop[9,23] gain increasing attention due to their higher chemical stability and durability stemming from Au component. However, the current preparation of CS Au-
60 Pt NDs is either implemented via a tedious two-step process or via a simple one-step process with rather broad size distribution.[9,24] Furthermore, the sizes of the Au-Pt NDs obtained so far are still large due to the use of large Au nanoparticles as seeds. For example, Yang and coworkers reported the synthesis
65 of Au-Pt bimetallic NDs with sizes of 22.6 nm *via* selective overgrowth of Pt on 11.4 nm multiply twinned Au seeds.[25] The catalyst size determines the specific surface area and the ratio of surface to bulk atoms. Although dendritic CS Au-Pt nanomaterials were also prepared on small Au NPs by two-step
70 method, however, the electrocatalytic performance (about 0.204 A mg$_{Pd}^{-1}$) is still to be improved for fuel cell due to dense branches on their surfaces.[26] Thus, it is technically favorable to synthesize the high quality CS Au-Pt NDs with sizes as small as possible in a facile and economic manner.
75 Recently, one become increasingly aware of the effects of surfactants,[27] used to stabilize nanoparticles and control their

morphology, on the nanoparticle catalytic activity. Since these capping agents are essential for the preparation, the tedious post-treatment process has to be conducted to remove the surfactants from the surfaces of the catalysts before the use of these catalysts. Herein, we present a simple and efficient strategy for high yield synthesis of well-dispersed, CS Au-Pt NDs *via* the overgrowth of platinum on *in situ* gold nanoparticles in aqueous media at room temperature. As-prepared NDs are marked as CS Au-Pt$_m$ NDs, where m represents the Pt-to-Au molar ratio used for the ND synthesis. Instead of additional pre-formed ones, Au nanoparticles *in situ* formed in the reaction media, were used as seeds for subsequent nucleation and growth of Pt nanobranches atop, resulting in CS Au–Pt$_5$ NDs with the sizes of about 14 nm. To our best knowledge, the resulting NDs should be the smallest compared to those reported in literature. The average dimension of the Pt nanobranches on the ND surfaces is about 2.6 nm × 4.2 nm. Due to the morphological features, as-prepared CS Au-Pt$_5$ NDs exhibit electrochemically active surface area as large as 35.2 m^2 g^{-1}. In comparison with commercial Pt black (0.12 A mg_{Pd}^{-1}), the resulting CS Au-Pt$_5$ NDs have superior catalytic activity towards methanol oxidation (0.45 A mg_{Pd}^{-1}) due to the electronic interaction between the Au cores and Pt nanobranches in bimetallic Au-Pt$_5$ NDs and the high fraction of atomic steps, kinks, and corner atoms on the surfaces of the Pt nanobranches.

2 Experimental section

2.1 Materials

Chloroauric acid tetrahydrate (HAuCl$_4$·4H$_2$O), trisodium citrate dihydrate (Na$_3$C$_6$H$_5$O$_7$·2H$_2$O) and ascorbic acid (AA) were purchased from Sinopharm Chemical Reagent Co. Ltd. Potassium tetrachloroplatinate(II) (K$_2$PtCl$_4$, 99%) and commercial Pt black (nominally 10% on carbon black) were purchased from Alfa Aesar (Tianjin, China). All glassware and stirring bars were cleaned with *aqua regia* (3:1 v/v HCl (37%): HNO$_3$ (65%) solutions) and then rinsed thoroughly with H$_2$O before use. (*Caution: aqua regia solutions are dangerous and should be used with extreme care; never store these solutions in closed containers.*) Water used in all experiments was prepared in a three-stage Millipore Milli-Q plus 185 purification system and had a resistivity higher than 18.2 MΩ cm.

2.2 Synthesis of CS Au-Pt$_m$ NDs

A typical procedure for synthesis of Au-Pt$_5$ NDs was as follows. Firstly, the aqueous solution of HAuCl$_4$ (0.50 mL, 25 mM) was added into the aqueous solution of sodium citrate (1.5 mL, 34 mM) at room temperature under stirring. Water (0.50 mL) was added to bring the volume of the citrate-HAuCl$_4$ premixture solution to 2.5 ml. After about 11 min incubation, the aqueous solution of K$_2$PtCl$_4$ (12.5 mL, 5.0 mM) was added into the citrate-HAuCl$_4$ premixture solution under stirring, followed by further 30 min incubation under stirring. After addition of the aqueous solution of ascorbic acid (AA) (2.0 mL, 0.25 M) into the citrate-HAuCl$_4$-K$_2$PtCl$_4$ solution during 3 h, CS Au-Pt$_5$ NDs were obtained. The final concentrations of K$_2$PtCl$_4$, HAuCl$_4$, citrate, and AA were 3.6, 0.70, 3.0, and 29.4 mM, respectively. The molar ratios of Pt-to-Au and AA-to-Pt were 5.0 and 8.0, respectively. The Au-Pt$_5$ NDs were separated and excess of AA was removed by repetition of centrifugation (at 10000 rcf for 10

min), supernatant decanting, and water washing for three times. Subsequently, the CS Au-Pt$_5$ NDs were redispersed in water with the help of sonication to make a colloidal suspension for further characterization.

2.3 Synthesis of spherical hyperbranched Pt particles

The spherical hyperbranched Pt particles were prepared according to a modified protocol reported in literature.[28] Typically, 2.5 mL of aqueous AA solution (0.10 M) was quickly added into 2.5 mL of aqueous K$_2$PtCl$_4$ solution (25 mM). The mixture solution was sonicated for 30 min. The hyperbranched Pt particles were separated and excessive AA was also removed by repetition of centrifugation (at 10000 rcf for 10 min), supernatant decanting, and water washing for three times. Finally, the resulting hyperbranched Pt particles were redispersed in water with the help of sonication to make a colloidal suspension for further characterization.

2.4 Characterizations

Transmission electron microscopy (TEM) and high-resolution TEM (HRTEM) images were obtained with a JEOL JEM-2100F transmission electron microscope operating at an acceleration voltage of 200 kV. Elemental mapping images were acquired by energy dispersive X-ray spectroscopy (EDS) using JEOL JEM-2100F electron microscope equipped with a STEM unit. X-Ray Photoelectron Spectroscopy (XPS) measurements were carried out on Thermo Fisher Scientic Escalab 250 XPS spectrometer, using Al Ka X-ray radiation for excitation.

2.5 Electrochemical measurements

Cyclic voltammetry (CV) and chronoamperomeric (CA) experiments were performed in a standard three-electrode cell in a CHI660D workstation at room temperature. A glassy carbon electrode (GCE) modified by as-prepared CS Au-Pt$_m$ NDs employed as the working electrode while an Ag/AgCl electrode and Pt wire were used as the reference electrode and auxiliary electrode, respectively. The bare GCE was polished successively with 0.3 and 0.05 μm alumina slurries, followed by rinsing thoroughly with pure water and drying at room temperature.

The typical procedure for the preparation of GCE modified by as-prepared CS Au-Pt$_m$ NDs was as follows. 12 μL of Au-Pt$_m$ ND solution was drop-coated on freshly prepared bare GCE, followed by drying in air. 10 μL of the ethanol solution of Nafion (0.2 wt %) was cast on the surface of the GCE coated by Au-Pt$_5$ NDs, followed by drying in air.

Cyclic voltammograms (CVs) used for determination of the electrochemically active surface area (ECSA) of Pt-based catalysts, were recorded between -0.2V and 1.2V in N$_2$-saturated 0.5 M H$_2$SO$_4$ solution with a scan rate of 50 mV/s. For methanol oxidation in acidic media, CVs were recorded between 0 V and 1.0 V in N$_2$-saturated 0.5 M H$_2$SO$_4$ and 1.0 M methanol solution at a scan rate of 20 mV/s. The ECSA was calculated by measuring the charge collected in the hydrogen adsorption/desorption region after double-layer correction and assuming a value of 0.21 mC cm^{-2} for the adsorption of a hydrogen monolayer.[29,30] Their specific current densities and mass current densities were normalized by their ECSAs and the loaded Pt amounts of each catalyst, respectively.

The CO stripping voltammetry was performed in 0.1 M H$_2$SO$_4$

solution. After purging the solution with ultrapure N_2 for 30 min, ultrapure CO gas was bubbled for 10 min under a fixed potential of -0.2 V vs Ag/AgCl, to promote the formation of a CO adlayer on the surface of the catalyst. Further, dissolved CO was flushed
5 out by purging the solution with ultrapure N2 for 30 min The CO stripping voltammetry patterns were recorded at a potential scan rate of 50 mV s−1.

3 Results and Discussion

3.1 Morphology of as-prepared Au-Pt$_5$ NDs

10 Fig. 1a shows the TEM image of CS Au-Pt$_5$ NDs obtained under optimal reaction conditions. The nanoparticles with of other shapes are hardly visible. These CS Au-Pt$_5$ NDs have uniform shape and narrow size distribution; the average size is about 14 nm. The average length and width of the small branches on the
15 ND surfaces are about 4.2 nm and 2.6 nm, respectively. These small branches are spatially separated from each other, which render these Au-Pt$_5$ NDs bearing maximumly accessible surface area.[19]
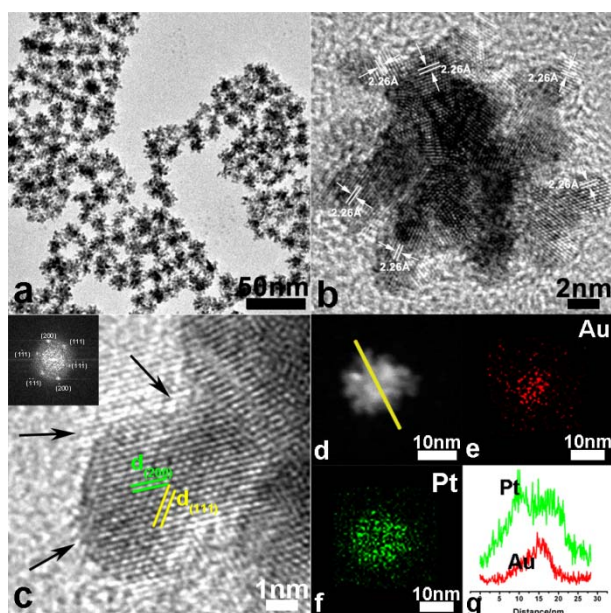

20 **Fig. 1** TEM (a) and HRTEM images (b and c) of Au-Pt$_5$ NDs, The atomic steps, kinks, and corner atoms on one single branch in the Au-Pt$_5$ ND are indicated by black arrows in the HRTEM image (c). The inset in Fig. 1c is the corresponding Fourier-transform (FT) pattern of the selected branch. HAADF-STEM-EDS mapping images (d, e and f) and cross-sectional
25 compositional line profile (g) of one single Au-Pt$_5$ ND. The concentrations of K_2PtCl_4, $HAuCl_4$, citrate, and AA are 3.6, 0.70, 3.0, and 29.4 mM, respectively. The molar ratios of Pt-to-Au and AA-to-Pt are 5.0 and 8.0, respectively.

The HRTEM image (Fig. 1b) of a single Au-Pt$_5$ ND shows the
30 lattice distances of the branches are about 0.226 nm, which is the typical d spacing of the (111) plane of face centered cubic (fcc) Pt. HRTEM image of a single branch of one Au-Pt$_5$ ND (Fig. 1c) clearly indicates the observed d spacings are the (111) and (200) planes of Pt, which is also in good agreement with the
35 corresponding Fourier-transform (FT) pattern (Fig. 1c, inset). It can be seen that a number of defects (such as atomic steps, kinks, and corner atoms) are present on the surfaces of the Pt branches (Fig. 1c and Fig. S1, ESI†), which can act as highly active sites

for catalysis.[31-34] Moreover, the ring patterns with intense spots in
40 the selected area electron diffraction (SAED) patterns (Fig. S2, ESI†) are assigned to (111), (200), (220), (311), and (400) planes of fcc Pt, respectively, indicating that the shells are composed of Pt. The HAADF-STEM-EDS mapping images (Figs.1d, 1e, and 1f) of one single Au-Pt$_5$ ND demonstrate that the nanodendrite is
45 composed of the elemental Au and Pt. In addition, Pt is distributed throughout the entire particle (Fig. 1e) while Au is mainly concentrated in the core region (Fig. 1f), confirming the CS structure feature of as-prepared Au-Pt$_5$ NDs. The CS structure is further confirmed by the EDS mapping of a patch of Au-Pt$_5$
50 NDs (Fig.S3, ESI†), which shows that each particle has an individual Au core and Pt shell. The cross-sectional compositional line profile of one single Au-Pt$_5$ ND (Fig. 1g) reveals that different from that of conventional CS structures, the line profile of the Au-Pt$_5$ ND show a noticeable valley, which is
55 attributed to dentritic structure. Therefore, the CS structured Au-Pt NDs were successfully obtained. In addition, the Pt-to-Au atomic ratio in the resulting Au-Pt$_5$ NDs is 4.6, which is rather close to the initial molar ratio of Pt-to-Au in the citrate-$HAuCl_4$-K_2PtCl_4 solution.

60 ### 3.2 Formation mechanism of CS Au-Pt$_5$ NDs

According to our experimental procedure, as depicted in scheme 1, the synthesis of CS Au-Pt$_m$ NDs involve three major steps: (a) mixing of $HAuCl_4$ and sodium citrate in water at room temperature under stirring; (b) formation of Au seeds upon
65 adding K_2PtCl_4 into the citrate-$HAuCl_4$ mixture solution under stirring, and (c) seeded growth of Au-Pt$_m$ NDs upon AA addition.
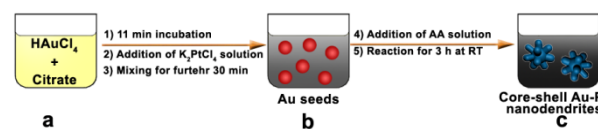
Scheme 1. Schematic depiction of synthetic procedure of CS Au-Pt NDs.

To shed light on the formation mechanism of CS Au–Pt$_5$ NDs,
70 a series of aliquots of the intermediate reaction solutions were extracted from the reaction mixtures at different reaction times for TEM characterization.
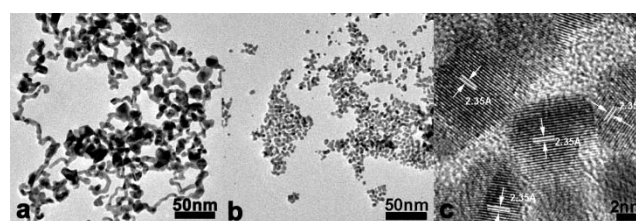

Fig. 2 TEM image (a) of nanowire-like Au nanoparticles obtained in
75 citrate-$HAuCl_4$ pre-mixture solution after 11 min incubation, TEM (b) and HRTEM images (c) of Au nanoparticles obtained in citrate-$HAuCl_4$-K_2PtCl_4 mixture solution before AA addition. The concentrations of K_2PtCl_4, $HAuCl_4$, and citrate are 4.2, 0.83, and 3.4 mM, respectively. The molar ratio of Pt-to-Au is 5.0.

80 After 11 min incubation of the citrate-$HAuCl_4$ premixture solution, the intermediate product is nanowire-like Au nanoparticles (Fig. 2a). After addition of K_2PtCl_4 into citrate-$HAuCl_4$ mixture solutions, followed by 30 min incubation, nearly quasi-spherical Au nanoparticles of about 5.5 nm in size are

gradually formed (Fig. 2b). These small Au nanoparticles tend to readily coalesce and fuse together during TEM characterization, indicating their high surface activity. The lattice distances of these nanoparticles in the HRTEM image (Fig. 2c) are 0.235 nm, which is in good agreement with the d spacing of the (111) plane of fcc Au. Fig. 3a shows that the Pt nanobranches immediately grow on the surfaces of the Au nanoparticles after AA addition (within 1 min); some Au nanoparticles with fewer branches can be clearly observed. The result indicates that Au nanoparticles act as seeds for growth of CS Au-Pt NDs. Within 5 min after AA addition, all Au nanoparticles are covered by Pt branches of different length and diameter (Fig. 3b). With the reaction further proceeding, the length and width of the Pt branches both increase; the average diameter of Au-Pt NDs also increase from 6.7 nm to 14 nm (Figs. 3a to 3d). Due to lattice mismatch, Pt can hardly grow uniformly on the surface of Au seed particles. 2,3-diketo-l-gulonic acid (DGA) from AA oxidation, serves as a shape-directing agent to direct the branched growth of Pt on Au seeds.[28] Moreover, the fast reduction rate of Pt by an autocatalytic process is also widely used to account for the formation of dendritic Pt branches[10,35] Furthermore, the Au seeds should provide the nucleation sites for Pt branches to grow in a spatially well separated manner to avoid overlap and fusion, thus leading to an open dendritic structure.[10]
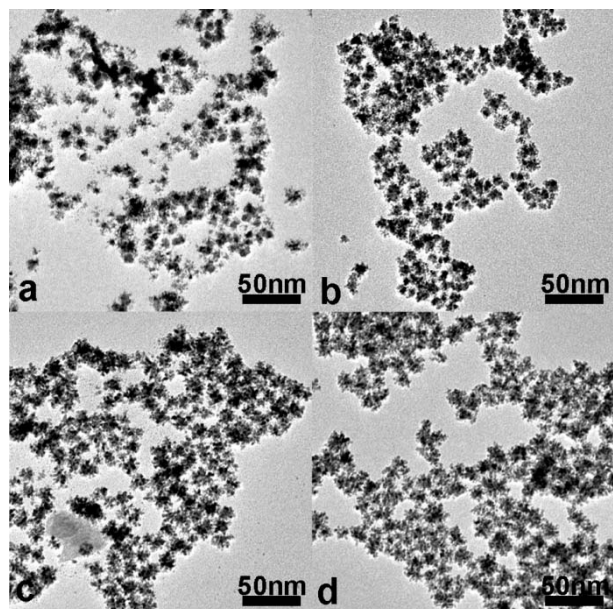

Fig. 3 TEM images of intermediate products extracted from the reaction mixture at different reaction times after AA addition: 1 min (a), 5 min (b), 30 min (c), and 3 h (d). The concentrations of K_2PtCl_4, $HAuCl_4$, citrate, and AA are 3.6, 0.70, 3.0, and 29.4 mM, respectively. The molar ratios of Pt-to-Au and AA-to-Pt are 5.0 and 8.0, respectively.

3.3 Effect of incubation time of citrate-$HAuCl_4$ premixture

In our previous work,[36-38] the Au nuclei can be formed during incubation of citrate-$HAuCl_4$ mixture at room temperature, which determines the amount of nuclei and the morphology. For synthesis of CS Au-Pt_5 NDs, the incubation time was tuned in the range of 9 to 18 min (Figs. S4a and S4b, ESI†). During this period, enough Au nuclei should be formed by citrate reduction of $HAuCl_4$.[39] Before addition of K_2PtCl_4 solution, nanowire-like Au nanoparticles are formed (Fig. 2a), and however, nearly quasi-

spherical Au nanoparticles are obtained after addition of K_2PtCl_4 solution (Fig. 2b). In the previous work reported by the Lee group, Au(0) atoms can be formed quickly by citrate reduction at high temperature, which lead to the transformation of wire-like to spherical morphology.[40] Thus, fast formation of Au(0) atoms is also necessary at room temperature in our case. Note that this shape transformation did not occur at room temperature in the absence of K_2PtCl_4 or when the aqueous solution of K_2PtCl_6 was added into the citrate-$HAuCl_4$ mixture solutions (Fig. S5, ESI†). This is because that on the basis of their reduction potential, Pt(II) ions are oxidized by Au(III) ions into Pt(IV) ions (Table S1, ESI†), thus leading to fast formation of Au(0) atoms and in turn facilitating nucleation. In contrast, Pt(IV) ions cannot be oxidized by Au(III) ions. Thus, the fast formation rate of Au(0) atoms by citrate reduction at room temperature is achieved by the additional K_2PtCl_4. As shown in Fig. 4, the morphology and dispersity of the Au seeds had a vital effect on the final morphology of Au-Pt products after AA addition. When the citrate-$HAuCl_4$ mixtures are incubated for 38 min, nanowire-like Au nanoparticles cannot be totally transformed into nearly quasi-spherical Au nanoparticles after addition of K_2PtCl_4 solution (Fig. 4a) possibly due to fusion and growth of Au nuclei by autocatalytic reaction.[41] In addition to a small amount of Au-Pt NDs, the short nanorod-like, hyperbranched Au-Pt products is obtained as byproduct as a result of the growth of Pt on bigger Au aggregates (Fig. 4c). When the incubation time is further extended to 68 min, short-rod-like Au nanoparticles and big Au nanoparticles are obtained (Fig. 4b), thus leading to the formation of spherical, hyperbranched Au-Pt products, which sizes are in the range of 20 to 100 nm (Fig. 4d).
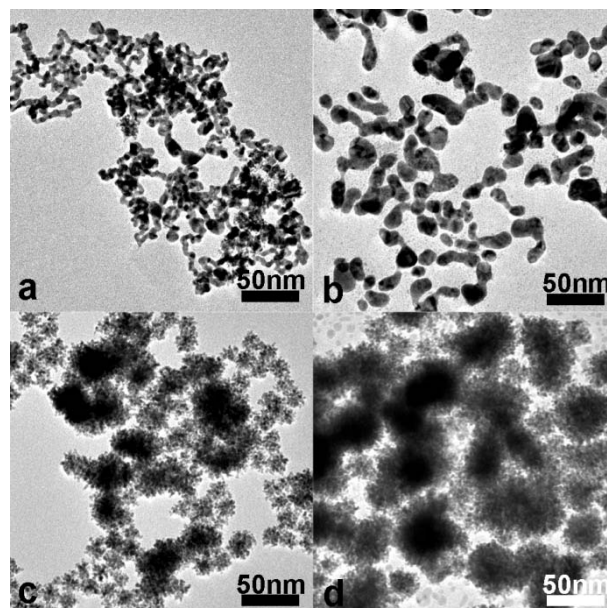
Fig. 4 TEM images of Au nanoparticles obtained after the citrate-$HAuCl_4$-K_2PtCl_4 mixture solution incubated for 38 min (a) and 68 min (b) before AA addition and the corresponding Au-Pt products (c) and (d). The concentrations of K_2PtCl_4, $HAuCl_4$, citrate, and AA are 3.6, 0.70, 3.0, and 29.4 mM, respectively. The molar ratios of Pt-to-Au and AA-to-Pt are 5.0 and 8.0, respectively.

3.4 Effect of the mixing time of citrate-$HAuCl_4$-K_2PtCl_4 solution before AA addition

As mentioned above, the formation of nearly quasi-spherical Au seeds is mainly due to the reaction between Pt(II) ions and Au(III) ions. Thus, the mixing time before AA addition also has an effect on the synthesis of CS Au-Pt NDs. It is known that AA can fast reduce Au(III) ions into Au(I) ions and further into Au atoms by autocatalytic reaction. Thus, the nanowire-like and dendritic structured Au nanoparticles are formed (Fig. 5a) if AA is quickly added shortly after K_2PtCl_4 addition (e.g. 30 s). Accordingly, the short nanorod-like and spherical, hyperbranched Au-Pt products dominate (Fig. 5c). In order to form nearly quasi-spherical Au nanoparticles the current work, AA solution should be added in to citrate-$HAuCl_4$-K_2PtCl_4 mixture solutions after the mixture solutions are incubated for 10 min (Fig. 5b), thus resulting in the fabrication of CS Au-Pt NDs with high quality (Fig. 5d).
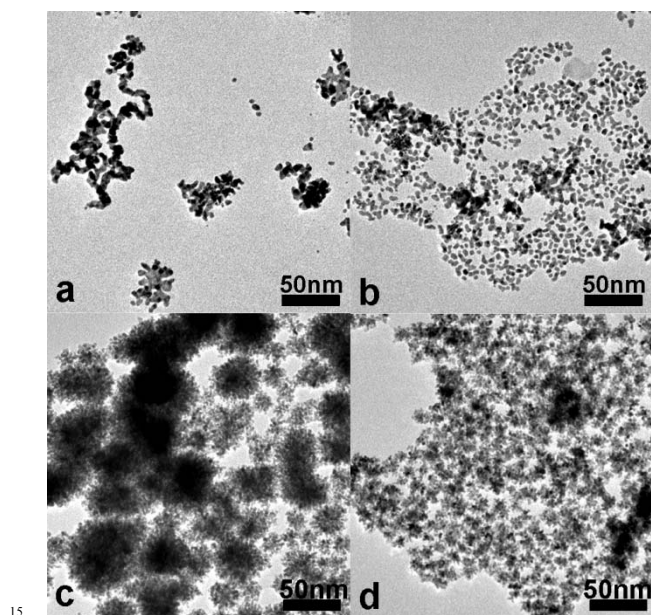
Fig. 5 TEM images of Au nanoparticles obtained after the citrate-$HAuCl_4$-K_2PtCl_4 solutions incubated for 30 s (a) and 10 min (b) before AA addition and the corresponding Au-Pt products (c) and (d). The concentrations of K_2PtCl_4, $HAuCl_4$, citrate, and AA are 3.6, 0.70, 3.0, and 29.4 mM, respectively. The molar ratios of Pt-to-Au and AA-to-Pt are 5.0 and 8.0, respectively.

3.5 Effect of the Pt-to-Au molar ratio on the morphology of Au-Pt products

The effect of Au-to-Pt molar ratios on the morphology of the CS Au-Pt NDs and corresponding electrocatalytic performance on methanol has been investigated in detail (Figs. 6 and 7). When the Pt-to-Au molar ratio is 1.0, the Au-Pt nanoparticles have irregular-shape and broad size distribution; the particle sizes are in the range of 3 to 11 nm (Fig. 6a). With the Pt-to-Au molar ratio increasing to about 2.5, smaller and fewer branches start to emerge on each Au-Pt nanoparticles; the particle sizes are in the range of 6 to 13 nm (Fig. 6b). When the Pt-to-Au molar ratio is slightly increases from 4.0 to 6.0, well-defined Au-Pt NDs with narrow size distribution were obtained and the average ND sizes increase from 11 to 14 and 16 nm (Figs. 6c, 1a, and 6d). The size increase of Au-Pt NDs can be attributed to the increase of the Pt amount used. These results indicate that finely tuning the Pt-to-Au molar ratio can produce well-defined Au-Pt products in high-quality.
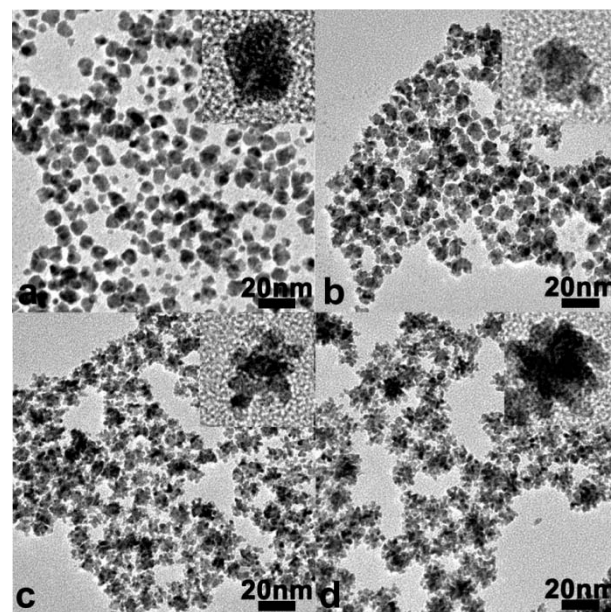
Fig. 6 TEM images of Au-Pt products obtained at different Pt-to-Au molar ratios: 1.0 (a), 2.5 (b), 4.0 (c), and 6.0 (d). The insets are the magnified images of corresponding single Au-Pt product. The concentrations of $HAuCl_4$ and citrate are 0.70 and 3.0 mM, respectively. The AA-to-Pt molar ratio is 8.0.

3.6 Electrochemical active surface area (ECSA) of Au-Pt products with different morphology
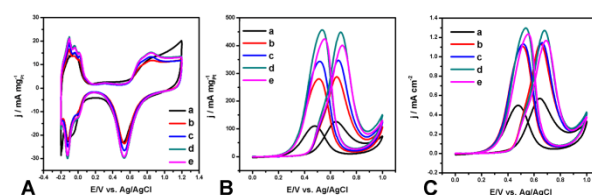

Fig. 7 CV curves (A, B, and C) of GCEs modified by Au-Pt_1 (a, black curve), Au-$Pt_{2.5}$ (b, red curve), Au-Pt_4 (c, blue curve), Au-Pt_5 (d, dark cyan curve), and Au-Pt_6 (e, magenta curve) measured in 0.50 M H_2SO_4 solution in the absence (A) and presence (B and C) of 1.0 M methanol, respectively. The currents are normalized by the Pt mass loaded on GCE (A and B) and ECSA values (C), respectively. The scan rates are 50 mV s^{-1} (A) and 20 mV s^{-1} (B and C), respectively. The concentrations of $HAuCl_4$ and citrate are 0.70 and 3.0 mM, respectively. The AA-to-Pt molar ratio is 8.0.

Pt catalysts with dendritic structure are expected to have high electrocatalytic performance on methanol oxidation due to their large electrochemical active surface area (ECSA). Here we tested all the Au-Pt_m products obtained and compare their performance in order to select the best catalyst. The ECSA values of Au-Pt_1, Au-$Pt_{2.5}$, Au-Pt_4, Au-Pt_5, and Au-Pt_6 NDs are calculated to be 22.2, 25.3, 30.3, 35.2, and 34.3 m^2 g^{-1}, respectively, by measuring the charge collected in the hydrogen adsorption/desorption region after double-layer correction in 0.5 M H_2SO_4 solution at room temperature at a scan rate of 50 mV·s^{-1} (Fig. 7A). Among the nanoparticles obtained, Au-Pt NDs have high ECSA values, which increases and then decrease with the Pt-to-Au molar ratio. As such, Au-Pt_5 NDs show the highest ECSA value. Fig. 7B depicts the CVs of the GCE modified by Au-Pt_1, Au-$Pt_{2.5}$, Au-Pt_4,

Au-Pt$_5$, and Au-Pt$_6$ products, respectively. Similarly, the GCE modified by Au-Pt$_5$ NDs exhibits the highest electrocatalytic activity by displaying highest mass normalized current density under the same conditions (Fig. 7B). The peak of the mass-normalized current density of Au-Pt$_5$ NDs (about 0.45A mg$_{Pd}$$^{-1}$) is about 3.6-fold larger than that of Au-Pt$_1$ nanoparticles without dendritic structure (about 0.13 A mg$_{Pd}$$^{-1}$) in the positive-going scan. The currents of these Au-Pt particles are also normalized with respect to the ECSA values to obtain their specific activity (Fig. 7C). The current density of the Au-Pt$_5$ NDs still is the largest (1.27 mA cm^{-2}), which is 2.2-fold larger that of Au-Pt$_1$ product without dendritic structure (0.57 mA cm^{-2}). All these results indicate that the Au-Pt$_5$ NDs have the best electrocatalytic performance for methanol oxidation (Table S2, ESI†).

3.7 Effect of the AA concentration on the morphology of Au-Pt$_5$ NDs and their ECSAs

In general, the excess amount of AA is used to prepare Pt dendrites.[28] However, we found that the AA concentration still had a slight effect on the morphology of Au-Pt$_5$ NDs (Fig. 8 and Table S3, ESI†). After careful assessment of Au-Pt$_5$ NDs in each TEM image, it is found that all Au-Pt$_5$ NDs have the similar sizes around 14 nm, while the length of the Pt nanobranches on the Au-Pt$_5$ NDs increases with the AA-to-Pt molar ratio with the width (about 2.6 nm) little changed; the maximum average length is about 4.2 nm obtained when the AA-to-Pt molar ratio is > 8.0. As expected, these Au-Pt$_5$ NDs obtained at the AA-to-Pt molar ratio of 8.0 show the highest ECSA (Fig. 8d).
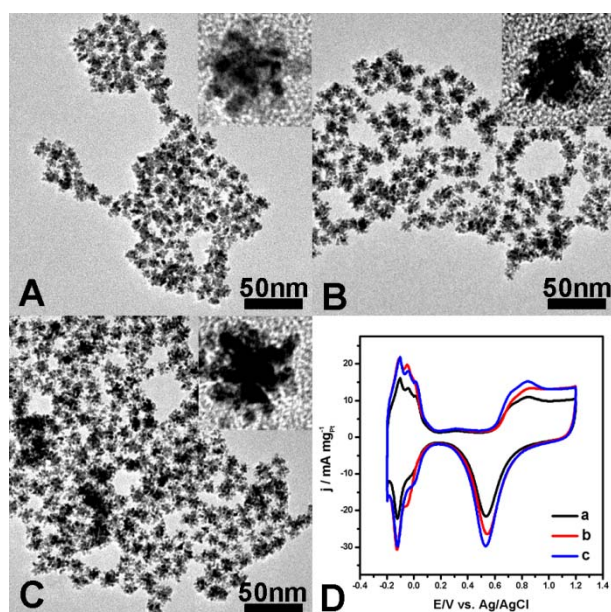
Fig. 8 TEM images (a, b, and c) of the Au-Pt$_5$ NDs obtained at different AA-to-Pt molar ratios: 2.0 (a), 4.0 (b), and 8.0 (c). CV curves (d) of the GCE modified by the resulting Au-Pt$_5$ NDs measured in 0.50 M H$_2$SO$_4$ solution at a scan rate of 50 mV s^{-1}. The currents of corresponding Au-Pt$_5$ NDs are normalized by the Pt mass loaded on GCE. The insets in (a, b, and c) are the high magnification TEM images of the corresponding one single Au-Pt$_5$ ND. The concentrations of K$_2$PtCl$_4$, HAuCl$_4$, and citrate are 3.6, 0.70, and 3.0 mM, respectively. The Pt-to-Au molar ratio is 5.0.

3.8 Electrocatalytic activity of Au-Pt$_5$ NDs for methanol oxidation

On the basis of the aforementioned results, the Au-Pt$_5$ NDs prepared at the AA-to-Pt molar ratio of 8.0 are the good candidate for catalysis of methanol oxidation. To investigate the potential use as the anodes of direct methanol fuel cells, the electrocatalytic performance of the Au-Pt$_5$ NDs on methanol oxidation was studied in detail and compared with those of commercial Pt black and spherical hyperbranched Pt particles[28] (Fig. S6, ESI†). The ECSA values of the Au-Pt$_5$ NDs, commercial Pt black and spherical hyperbranched Pt particles are calculated by measuring the charge collected in the hydrogen adsorption/desorption region after double-layer correction (Fig. 9A). The ECSA of the GCE modified by Au-Pt$_5$ NDs (35.2 m^2 g^{-1}) is about 2.35 times higher than that of hyperbranched Pt nanoparticles (15.0 m^2 g^{-1}) and 2.5 times higher than that of commercial Pt black electrode (14.1 m^2 g^{-1}), respectively. Fig. 9B depicts the CVs of GCE modified by commercial Pt black, spherical hyperbranched Pt nanoparticles and Au-Pt$_5$ NDs, respectively. The mass-normalized current density of Au-Pt$_5$ NDs (about 0.45 A mg$_{Pd}$$^{-1}$) is about 2.3-fold and 3.8-fold higher than that of spherical hyperbranched Pt particles (0.20 A mg$_{Pd}$$^{-1}$) and the commercial Pt black (0.12 A mg$_{Pd}$$^{-1}$) in the positive-going scan, respectively. These results should be attributed to the multi-nanobranch-structure (2.6 nm × 4.2 nm) and the ultrasmall size (ca. 14 nm) of as-prepared Au-Pt$_5$ NDs. They also underline excellent electrochemical accessibility, which is of great importance for electrocatalytic reactions. In order to assess the specific activity of Au-Pt$_5$ NDs, hyperbranched Pt particles and commercial Pt black, the currents of their modified GCEs were also normalized by the ECSA values (Fig. S7, ESI†). The current density of Au-Pt$_5$ NPs (1.28 mA cm^{-2}) is comparable to that of hyperbranched Pt particles (1.33 mA cm^{-2}) as hyperbranched Pt particles bear a smaller ECSA. However, the current density of Au-Pt$_5$ NPs is higher than that of commercial Pt black (0.84 mA cm^{-2}) or commercial Pt/C catalyst from E-TEK (1.05 mA cm^{-2}).[42] The comparison in current densities indicated that the Au–Pt$_5$ NDs showed a higher specific activity than that of commercial Pt/C catalyst (E-TEK) or the commercial Pt black.
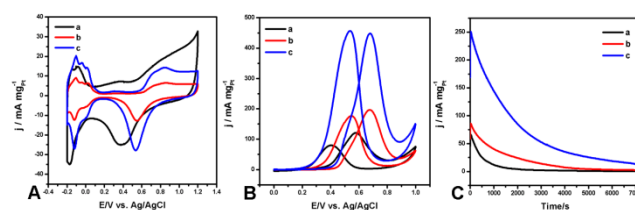
Fig. 9 CV curves (A and B) and CA curves (C) of GCE modified by commercial Pt black (a, black curve), hyperbranched Pt nanoparticles (b, red curve), and Au-Pt$_5$ NDs (c, blue curve) measured in 0.50 M H$_2$SO$_4$ solution in the absence (A) and presence (B and C) of 1.0 M methanol. The scan rates of (A) and (B and C) are 50 mV s^{-1} and 20 mV s^{-1}, respectively. CA curves (C) are recorded at 0.50 V. The currents are normalized by the Pt mass loaded.

To demonstrate the durability of the catalytic performances, the long-term oxidation of methanol by commercial Pt black, spherical hyperbranched Pt particles and Au-Pt$_5$ NDs were performed, respectively. On the basis of their chronoamperometric (CA) curves, the electrochemical stability of the Au-Pt$_5$ NDs is superior to that of the spherical hyperbranched Pt nanoparticles or commercial Pt black (Fig. 9C). The oxidation

current of the spherical hyperbranched Pt nanoparticles is a little better than commercial Pt black and not comparable to that of the Au-Pt$_5$ NDs. The oxidation current of the Au-Pt$_5$ NDs is higher than that of the spherical hyperbranched Pt particles or commercial Pt black in the entire time range and the current decay is also slower than that of the spherical hyperbranched Pt particles or commercial Pt black. These results suggest that the Au-Pt$_5$ NDs have a long-term high electrocatalytic activity for methanol oxidation in acid media.

In comparison with commercial Pt black, the higher catalytic performance of Au-Pt$_5$ NDs on methanol oxidation may be the attributed to their core-shell structure and multi-branched feature. The presence of the Au core in each Au-Pt ND not only facilitates the growth of the Pt branches but also plays a key role in the enhanced activity of the Au-Pt NDs relative to pure hyperbranched Pt particles due to the d-center theory.[43] On the basis of the electronegativity difference between Au and Pt (2.54 and 2.28, respectively), the potential electron-withdrawing effect from Au to the neighboring Pt may induce an increase of 5d vacancies in Pt, thus significantly improving the adsorption of methanol on the surface of Pt sites and thus favoring the methanol oxidation.[44] X-ray photoelectron spectroscopy (XPS) was further used to investigate the valence states of Pt in spherical hyperbranched Pt particles and Au-Pt$_5$ NDs (Fig. S8, ESI†). As expected, one can see that Pt $4f_{7/2}$ and $4f_{5/2}$ binding energies of the Au-Pt$_5$ NDs are 71.1 and 74.45 eV, respectively. The Pt 4f signal consisted of two pairs of Pt peaks. The most intense peaks (71.05 and 74.4 eV) were attributed to Pt (0). Compared with the Pt $4f_{7/2}$ and $4f_{5/2}$ binding energies of hyperbranched Pt particles (70.9 and 74.2 eV), a slight shift to higher values (about 0.15 eV) was observed in Au-Pt$_5$ NDs, suggesting that electrons indeed were transferred from Pt shell to Au cores. This result is attributed to the fact the thick Pt shells on the small Au cores weaken the electron-withdrawing effect. In addition, the abundant atomic steps, edges, and corner atoms in the Pt nanobranches of the Au–Pt$_5$ NDs also act as highly active sites for methanol oxidation.[25,34,45] More importantly, these active sites can tolerate undesirable agglomeration due to the special dendritic structure. Thus, the superior electrocatalytic activity of the bimetallic Au-Pt catalysts for methanol oxidation was achieved through strucure densign with proper Pt-to-Au molar ratio.

To understand the structure and morphology effect of Au-Pt NDs on the CO electrooxidation efficiency, a series of CO-stripping voltammetry was performed (Fig. S9, ESI†). The strong stripping peak of CO on the electrode modified by Au-Pt$_5$ NDs is centered at 0.52V, which is rather close to that of other Au-Pt NDs. However, it is 10 mV, and 160 mV more negative than those on the electrode modified by hyperbranched Pt particles and Pt black, respectively. This suggests that CO can be more easily oxidized on Au-Pt$_5$ NDs, indicating that the bifunctional mechanism may play more important role than the electronic effect arising from the increase of 5d vacancies, and the improved electrocatalytic activities of Au-Pt$_5$ NDs could be explained bifunctional mechanism.[46]

The potential cycling stability of GCEs modified by Au–Pt$_5$ NDs and commercial Pt black are also compared by using CV cycling (Fig. S10, ESI†). It can be seen that the oxidation peak current density of GCEs modified Au–Pt$_5$ NDs is reduced to about 20% while that of commercial Pt black is reduced to about 42% after 500 cycles of electrochemical oxidation of ethanol. The decrease in the current density of Au–Pt$_5$ NDs is attributed to the fact that the atomic steps, kinks, and corner atoms on the surfaces of the Pt branches disappear gradually and sinter together to form smooth surfaces during cycling stability test (Fig. S11, ESI†). However, the remaining current density (0.09 A mg$_{Pd}^{-1}$) of Au–Pt$_5$ NDs is still comparable to the original current density of commercial Pt black (0.12 A mg$_{Pd}^{-1}$). Thus, the stability of our Au-Pt NDs is still needed to improve in order to achieve their application in fuel cells.

Conclusions

In summary, a simple and efficient strategy has been developed for synthesis of well-dispersed, CS Au-Pt$_5$ NDs *via* overgrowth of platinum on gold nanoparticles *in situ* formed in water at room temperature. After optimization of the reaction conditions such as incubation time of citrate-HAuCl$_4$ solution, the mixing time of citrate-HAuCl$_4$-K$_2$PtCl$_4$ solution before AA addition, Pt-to-Au and AA-to-Pt molar ratios, Au-Pt$_5$ NDs with the superior catalytic performance can be obtained at high yield. They have uniform CS, dendritic shape, and narrowly distributed size; the average size is about 14 nm and the average dimension of the Pt nanobranches is about 2.6 nm × 4.2 nm. This unique structural feature renders the resulting Au-Pt$_5$ NDs with significantly increased electrochemically active surface areas. In comparison with commercial Pt black (0.12 A mg$_{Pd}^{-1}$), the Au-Pt$_5$ NDs have superior catalytic activity towards methanol oxidation (0.45 A mg$_{Pd}^{-1}$) due to the electronic interaction between the Au cores and Pt branches in bimetallic Au-Pt$_5$ NDs and high ratio of atomic steps, kinks, and corner atoms on the surfaces of the Pt branches.

Notes and references

[a]*State Key Laboratory of Crystal Materials, Shandong University, Jinan, 250100, P. R China. E-mail: hbxia@sdu.edu.cn*
[b]*Ian Wark Research Institute, University of South Australia, Adelaide, SA 5095, Australia*

† Electronic Supplementary Information (ESI) available: [Selected area electron diffraction (SAED) pattern, HRTEM, TEM and HAADF-STEM-EDS mapping images of the CS Au-Pt$_5$ NDs, TEM image of nanowire-like Au nanoparticles extracted from the citrate-HAuCl$_4$-K$_2$PtCl$_6$ solution with 11 min incubation, TEM images of other Au-Pt$_5$ NDs obtained with incubation of 9 min and 18 min, TEM image of the hyperbranched Pt particles, Table S1 for Summary of the redox potential values of half-reaction of AuCl$_4^-$/Au^0 and PtCl$_6^{2-}$/ PtCl$_4^{2-}$, Table S2 for summary of ECSAs, current densities normalized by mass and current densities normalized by ECSA of GCE modified by Au-Pt products, and Table S3 for summary of the lengths and widths of the branches on Au-Pt$_5$ NDs

prepared   under   different   AA-to-Pt   molar   ratios.].   See DOI:10.1039/b000000x/

1   B. Y. Xia, H. B. Wu, X. Wang and X. W. Lou, *Angew. Chem. Int. Ed.*, 2013, **52**, 12337-12340.

2.   X. L. Sun, D. G. Li, Y. Ding, W. L. Zhu, S. J. Guo, Z. L. Wang and S. H. Sun, *J. Am. Chem. Soc.*, 2014, **136**, 5745-5749.

3.   B. Y. Xia, H. B. Wu, Y. Yan, X. W. Lou and X. Wang, *J. Am. Chem. Soc.*, 2013, **135**, 9480-9485.

4.   C. H. Cui and S. H. Yu, *Acc. Chem. Res.*, 2013, **46**, 1427-1437.

5.   L. Kuai, S. Wang and B. Geng, *Chem. Commun.*, 2011, **47**, 6093-6095.

6.   Y. Xu and B. Zhang, *Chem. Soc. Rev.*, 2014, **43**, 2439-2450.

7.   B. Y. Xia, H. B. Wu, X. Wang and X. W. Lou, *J. Am. Chem. Soc.*, 2012, **134**, 13934-13937.

8.   S. Guo, S. Zhang and S. Sun, *Angew. Chem. Int. Ed.*, 2013, **52**, 8526-8544.

9.   H. Ataee-Esfahani, L. Wang and Y. Yamauchi, *Chem. Commun.*, 2010, **46**, 3684-3686.

10. B. Lim, M. Jiang, P. H. Camargo, E. C. Cho, J. Tao, X. Lu, Y. Zhu and Y. Xia, *Science*, 2009, **324**, 1302-1305.

11. Y. G. Guo, J. S. Hu, H. M. Zhang, H. P. Liang, L. J. Wan and C. L. Bai, *Adv. Mater.*, 2005, **17**, 746-750.

12. N. S. Porter, H. Wu, Z. Quan and J. Fang, *Acc. Chem. Res.*, 2013, **46**, 1867-1877.

13. D. S. Wang, P. Zhao and Y. D. Li, *Sci Rep*, 2011, **1**, 37.

14. Q. Yuan, Z. Y. Zhou, J. Zhuang and X. Wang, *Chem. Mater.*, 2010, **22**, 2395-2402.

15. L. Wang, M. Imura and Y. Yamauchi, *ACS Appl. Mater. Interfaces*, 2012, **4**, 2865-2869.

16. L. Wang and Y. Yamauchi, *J. Am. Chem. Soc.*, 2009, **131**, 9152-9153.

17   B. Y. Xia, Y. Yan, X. Wang and X. W. Lou, *Materials Horizons*, 2014, **1**, 379.

18. L. Wang and Y. Yamauchi, *Chem. Mater.*, 2009, **21**, 3562-3569.

19. L. Wang, Y. Nemoto and Y. Yamauchi, *J. Am. Chem. Soc.*, 2011, **133**, 9674-9677.

20. L. Wang and Y. Yamauchi, *J. Am. Chem. Soc.*, 2013, **135**, 16762-16765.

21. H. Ataee-Esfahani, M. Imura and Y. Yamauchi, *Angew. Chem. Int. Ed.*, 2013, **52**, 13611-13615.

22. L. Wang and Y. Yamauchi, *Chem. Mater.*, 2011, 23, 2457-2465.

23. J. Zhang, K. Sasaki, E. Sutter and R. R. Adzic, *Science*, 2007, **315**, 220-222.

24. S. J. Guo, J. Li, S. J. Dong and E. K. Wang, *J. Phys. Chem. C,* 2010, **114**, 15337-15342.

25. Y. Feng, H. Liu and J. Yang, *J. Mater. Chem. A*, 2014, **2**, 6130-6137.

26. S. Y. Wang, N. Kristian, S. P. Jiang and X. Wang, *Nanotechnology*, 2009, **20**, 025605.

27   S. Wang, L. Kuai, Y. Huang, X. Yu, Y. Liu, W. Li, L. Chen and B. Geng, *Chem. Eur. J.*, 2013, **19**, 240-248.

28. L. Wang, C. P. Hu, Y. Nemoto, Y. Tateyama and Y. Yamauchi, *Cryst. Growth Des.*, 2010, **10**, 3454-3460.

29. W. Sheng, H. A. Gasteiger and Y. Shao-Horn, *J. Electrochem. Soc.*, 2010, **157**, B1529-B1536.

30. K. J. J. Mayrhofer, D. Strmcnik, B. B. Blizanac, V. Stamenkovic, M. Arenz and N. M. Markovic, *Electrochim. Acta,*2008, **53**, 3181-3188.

31. S. W. Lee, S. Chen, W. Sheng, N. Yabuuchi, Y. T. Kim, T. Mitani, E. Vescovo and Y. Shao-Horn, *J. Am. Chem. Soc.*, 2009, **131**, 15669-15677.

32. N. Tian, Z. Y. Zhou, S. G. Sun, Y. Ding and Z. L. Wang, *Science*, 2007, **316**, 732-735.

33. Z. Y. Zhou, Z. Z. Huang, D. J. Chen, Q. Wang, N. Tian and S. G. Sun, *Angew. Chem. Int. Ed.*, 2010, **49**, 411-414.

34. H. B. Xia, Y. Ran, H. S. Li, X. T. Tao and D. Y. Wang, *J. Mater. Chem. A*, 2013, **1**, 4678-4684.

35. Y. J. Song, Y. Yang, C. J. Medforth, E. Pereira, A. K. Singh, H. Xu, Y. Jiang, C. J. Brinker, F. van Swol and J. A. Shelnutt, *J. Am. Chem. Soc.*, 2004, **126**, 635-645.

36. H. B. Xia, S. Bai, J. Hartmann and D. Y. Wang, *Langmuir*, 2010, **26**, 3585-3589.

37. W. C. Ding, Y. Liu, Y. J. Li, Q. R. Shi, H. S. Li, H. B. Xia, D. Y. Wang and X. T. Tao, *RSC Advances*, 2014, **4**, 22651-22659.

38. P. N. Zhang, C. X. Xi, C. Feng, H. B. Xia, D. Y. Wang and X. T. Tao, *CrystEngComm*, 2014, **16**, 5268-5274.

39. J. Turkevich, P. C. Stevenson and J. A. Hillier, *Discuss. Faraday Soc.*, 1951, **11**, 55-75.

40. B. K. Pong, H. I. Elim, J. X. Chong, W. Ji, B. L. Trout and J. Y. Lee, *J. Phys. Chem. C* 2007 **111**, 6281-6287

41   X. Ji, X. Song, J. Li, Y. Bai, W. Yang and X. Peng, *J. Am. Chem. Soc.*, 2007, **129**, 13939-13948.

42. A. B. A. A. Nassr, I. Sinev, M.-M. Pohl, W. Grünert and M. Bron, *ACS Catalysis*, 2014, **4**, 2449-2462.

43. B. Hammer and J. K. Norskov, *Adv. Catal.*, 2000, **45**, 71-129.

44. X. G. Ding, Y. Zou, F. Ye, J. Yang and J. Jiang, *J. Mater. Chem. A*, 2013, **1**, 11880-11886.

45.   M. A. Mahmoud, C. E. Tabor, M. A. El-Sayed, Y. Ding and Z. L. Wang, *J. Am. Chem. Soc.*, 2008, **130**, 4590-4591.

46. A. Chen and P. Holt-Hindle, *Chem. Rev* , 2010, **110**, 3767-3804.